J Mater Sci: Mater Med (2009) 20:1409–1418
DOI 10.1007/s10856-009-3711-7

# Development of nano-macroporous soda-lime phosphofluorosilicate bioactive glass and glass-ceramics

**H. M. M. Moawad · H. Jain**

Received: 27 November 2008 / Accepted: 6 February 2009 / Published online: 28 February 2009


**Abstract** We have extended the usefulness of bioactive glass-ceramics for the repair and reconstruction of hard tissues by introducing F ions that are known to be beneficial, especially in dentistry. Nano-macro multimodal porosity in soda-lime phosphofluorosilicate bulk samples was introduced by the recently developed melt-quench-heat-etch method. The choice of starting glass composition is based on $48SiO_2$–$2.7P_2O_5$–$xCaF_2$–$yCaO$–$zNa_2O$ where $x = 0, 1, 4, 8, 10, 12$, and $(y + z) = 49.3 - x$ (mol%). The effect of thermal and chemical treatment on the microstructure of samples is characterized by SEM, XRD and EDX. We find the formation of many crystalline phases, but mainly sodium calcium silicate, calcium phosphate, fluorapatite and calcium silicate. The bioactivity of soda-lime phosphofluorosilicate glass-ceramics is assessed by monitoring the formation of hydroxyl apatite (HA) layer: fluorapatite phase accelerates the rate of HA layer formation; the initial composition and multi-modal porosity are other key parameters that impact the formation of HA. The present porous glass-ceramics should be superior candidates for use in dental bone regeneration.

## 1 Introduction

Bone regeneration is required in many clinical treatments addressed by orthopedic and dental medicine. Bioactive glasses and bioactive glass-ceramics are the most suitable materials for the repair and reconstruction of diseased hard (bones and teeth) tissues [1, 2]. They have been proven to be more biocompatible than metals and fine ceramics. It has been shown that these materials firmly attach to bone by the formation of apatite-like surface layer [3]. So there has been increasing interest in the development of bioactive glass and glass-ceramics in relation to their chemical composition and microstructure [4, 5].

Basically, the physical and mechanical properties affect the active functional characteristic of most implants. On the other hand, the biological and chemical properties control an implant's ability to maintain its functionality throughout its use. Natural bones and teeth are multiphase, multifunctional materials, thus their overall properties are likely to be reproduced by multiphase synthetic materials. Most previous studies were directed to a single phase glass composition or one glass-ceramic. In general, bioactive glasses have poor mechanical properties, which have limited their applications to non-load bearing implants [6]. To improve mechanical properties, different bioactive glass-ceramics obtained by thermal treatment of glasses have been reported [7, 8]. However, there is unclear understanding of the effect of crystallization on the biological performance of glass-ceramics. Most simply, the bioactivity of a glass has been measured by the rate of hydroxy apatite (HA) formation in simulated body fluid (SBF). Various authors have reported contradictory observations that crystallization of bioactive glasses has adverse, little or no adverse effect on the bioactivity. For example, Li et al. [9] have shown that a bioactive glass can be transformed into an inert glass-ceramic, as the mechanical properties were enhanced. In contrast, Peitl et al. [10] have shown that crystallization of Hench's bioactive glass composition does not inhibit HA formation in an in vitro test even with a fully crystallized glass-ceramic. Vallet-Regi et al. [11] reported that crystallization of $SiO_2$–$CaO$–$P_2O_5$ bioactive

H. M. M. Moawad · H. Jain (✉)
Department of Materials Science and Engineering,
Lehigh University, Bethlehem, PA 18015, USA
e-mail: h.jain@lehigh.edu

glasses has no adverse effect on their bioactivity. Moawad and Jain [12] have shown that crystallization of soda-lime phosphosilicate bioactive glass accelerates HA formation in an in-vitro test.

The bioactive glass and glass-ceramics are also suitable as scaffold that enhances the body's own reparative capacity. A bone scaffold should serve as a template and support tissue growth. Ideally, it should show interconnected nano-macroporous structure similar to that of natural bone. This type of porous network is important for the following reasons [13]: (a) macropores ($\sim$100 μm) are important to enable tissue ingrowth and nutrient delivery to the center of the regenerated tissue and (b) nano-pores ($\leq$50 nm) are useful to promote cell adhesion, adsorption of biologic metabolites, and resorbability at controlled rates to match that of tissue repair. Recently, different methods have been developed for fabricating nano-macroporous bioactive glass and glass-ceramics, but the role of such microstructure on HA formation has not been established [12, 14–17].

Fluoride ions are usually added to drinking water and fluoride toothpastes. In addition, a crystal structure of fluorapatite ($Ca_5(PO_4)_3F$) is very similar to the crystal structure of hydroxy apatite ($Ca_5(PO_4)_3(OH)$). For all these reasons we have attempted to extend the usefulness of the soda lime phosphosilicate bioactive glass series by doping it with $CaF_2$ as a source of fluoride ions. In this study, glasses of the soda lime phosphofluorosilicate system were prepared and explored for their crystallization behavior by controlled heat treatment. Next, processing conditions were determined to introduce interconnected, crack-free multimodal porosity in the glass by the melt-quench-heat-etch (MQHEtch) method [14]. Finally, to assess bioactivity the formation of HA layer was determined in relation to morphology, texture, composition, and processing conditions.

## 2 Experimental procedure

The glasses of composition $48SiO_2$–$2.7P_2O_5$–$xCaF_2$–$yCaO$–$zNa_2O$, where $x = 0, 1, 4, 8, 10, 12$, $y + z = 49.3 - x$ (mol%), were prepared with $SiO_2$ (99.99%), $CaCO_3$ (99%), $Na_2CO_3$ (99%), $Ca_5(OH)(PO_4)_3$ (99%) and $CaF_2$ (99%) as starting materials. The calculated batch of powders was mixed and ground using an alumina mortar and pestle. It was melted in a platinum crucible at 1300°C for 2 h. The homogenized melt was poured into a stainless steel mold and then the so formed glass was annealed at 500°C to relax residual stresses. The result was a glass phase-separated on nanometer scale with interconnected spinodal texture. To induce additional larger scale phase separation, the samples were subjected further to a devitrification heat treatment in two steps: (a) nucleation step at $T_n$, which included heating at 3°C/min to 670°C and holding there for 1 h, and (b) crystal growth step at $T_x$, which included heating at the same rate to either 750°C or 1075°C and holding there for 6 h. Table 1 describes the temperature and time of heat treatment schedule. To create nano-macro porosity, the heat treated glasses were leached for 1 h in 0.3 N HCl at 85°C.

To identify the phases and observe microstructure the samples were analyzed by X-ray diffraction (XRD) and scanning electron microscopy (SEM). Hitachi 4300 Field Emission SEM was used to examine sectioned and polished samples of each glass to elucidate the phase separation and microstructure. To avoid charging, the SEM samples were coated with carbon. The elemental distribution in different phases was determined by Energy Dispersive X-ray (EDX) spectroscopy device attached to the SEM- Hitachi 4300. EDX spectra were calibrated by Cu K and Cu L as reference for peak position, and collected by using an area scan of image with EDAX-Genesis software package. The parameters for data acquisition (time, full scale for intensity, pulse processing time) were kept the same for all the samples. The pore size distribution of the samples was determined by mercury porosimeter (Micromeritics Auto pore IV).

The in vitro formation of apatite layer was observed in SBF, where the fluid contained inorganic ions in concentration corresponding to human blood plasma. The SBF was prepared by dissolving reagent grade NaCl, $NaHCO_3$, KCl, $K_2HPO_4 \cdot 3H_2O$, $MgCl_2 \cdot 6H_2O$, $CaCl_2 \cdot 2H_2O$, and $Na_2SO_4$ in deionized water [18]. The fluid was buffered at physiological pH of 7.4 at 37°C. Each glass or glass-ceramic specimen (2 mg) was immersed in 1 ml of SBF in a polyethylene bottle covered with a tight lid. The HA layer

**Table 1** Temperature and time of heat treatment schedule of various glasses in the $48SiO_2$–$2.7P_2O_5$–$xCaF_2$–$yCaO$–$zNa_2O$ (mol%) series with ($x = 1, 4, 8, 10, 12$) ($y + z = 49.3 - x$)

| $48SiO_2$, $xCaF_2$ (mol%) | Sample ID | Crystal growth temperature, $T_x$ (°C) |
|---|---|---|
| 48S glass | 48S | No heat treatment |
| 48S1F | 48S1FGI | 750 |
| 48S4F | 48S4FGI | 750 |
| 48S8F | 48S8FGI | 750 |
| 48S10F | 48S10FGI | 750 |
| 48S12F | 48S12FGI | 750 |
| 48S1F | 48S1FGII | 1075 |
| 48S4F | 48S4FGII | 1075 |
| 48S8F | 48S8FGII | 1075 |
| 48S10F | 48S10FGII | 1075 |
| 48S12F | 48S12FGII | 1075 |

All samples were given the same nucleation heat treatment

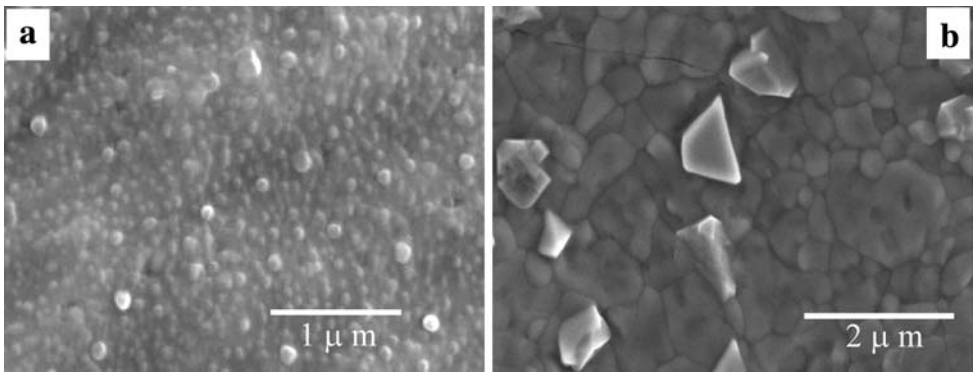


**Fig. 1** SEM micrographs of the glass-ceramic specimens to demonstrate the effect of growth temperature on microstructure: **a** 48S12FGI treated at 750°C, **b** 48S12FGII treated at 1075°C

formed on the surface of the glass-ceramics and porous glass-ceramic samples after soaking in SBF for 3 days was characterized by SEM, XRD and EDX. In addition, mid infrared spectra were obtained in reflectance mode, using Varian 7000e FT-IR spectrometer with KBR beam splitter and a GTGS detector, to characterize the HA layer formed on the surface of the porous glass-ceramic 48S4FGI sample after soaking in SBF for 1, 3 or 7 days. Also, the HA layer formed on the surface of the glass with and without $CaF_2$ after soaking in SBF for 7 days was characterized by XRD.

## 3 Results and discussion

### 3.1 Microstructure as a function of composition and heat treatment

Typical microstructures of 48SxFGI[1] and 48SxFGII glass series are shown in Fig. 1 for samples containing 12 mol% $CaF_2$, as examples of our glass-ceramics (see Table 1 for the description of all samples), which were subjected to two different growth heat treatments at 750 and 1075°C, as described above. It is clear from a comparison of the microstructures of the two glass-ceramic samples with the same $x$ value (Fig. 1) that the crystallite size increases with the growth temperature, $T_x$. Micrographs of all other samples in the 48SxFGI and 48SxFGII heat treated series also confirm that the heat treatment causes formation, growth and coalescence of the crystalline grains [19].

The XRD patterns of 48SxFGI and 48SxFGII glass samples, which were subjected to crystal growth heat treatments at 750 and 1075°C, are shown in Fig. 2I and II, respectively. The crystalline phases are identified as $Ca_4P_6O_{19}$, $Na_2Ca_2Si_3O_9$, $Na_2CaSi_3O_8$, $Ca_5(PO_4)_3F$ and $Ca_5Si_2O_8F_2$. The location of diffraction peaks matches the standard powder diffraction file (PDF) card numbers

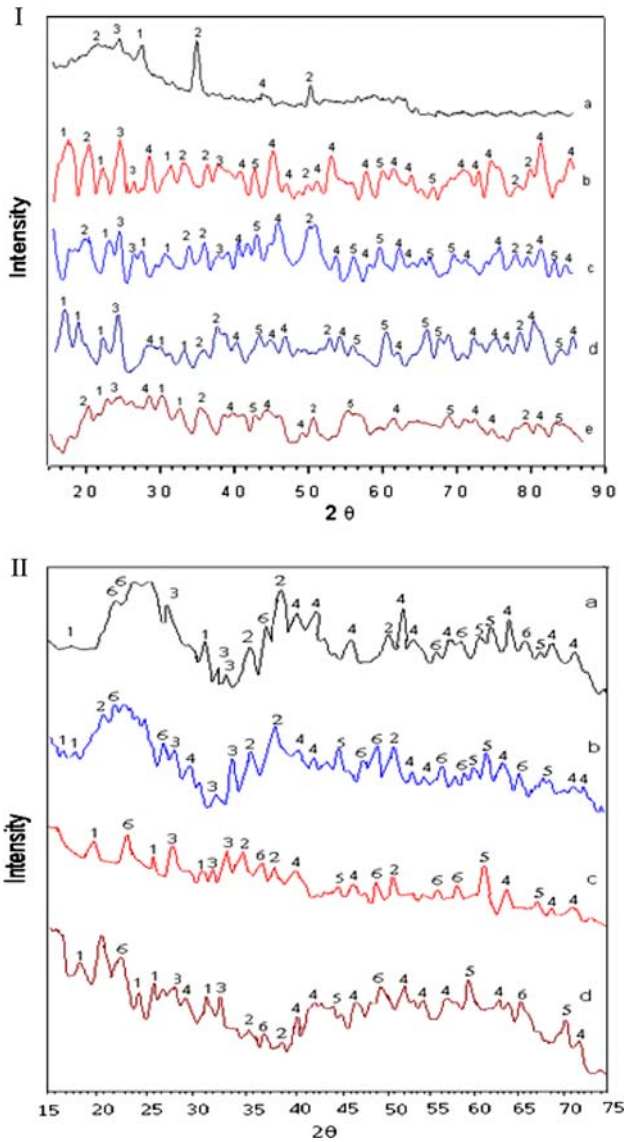


**Fig. 2** X-ray diffraction patterns of glass-ceramic samples after the nucleation and growth heat treatments: **I**: (a) 48S1FGI, (b) 48S4FGI, (c) 48S8FGI, (d) 48S10FGI, (e) 48S12FGI. **II**: (a) 48S4FGII, (b) 48S8FGII, (c) 48S10FGII, (d) 48S12FGII. The source of diffraction peaks: (1) $Ca_4P_6O_{19}$, (2) $Na_2Ca_2Si_3O_9$, (3) $Na_2CaSi_3O_8$, (4) $Ca_5(PO_4)_3F$, (5) $Ca_5Si_2O_8F_2$, (6) $CaSiO_3$

[1] The sample ID indicates that the starting batch was made of 48 mol% $SiO_2$and contained $x$ mol% of $CaF_2$. GI and GII refer to two growth temperatures of 750 or 1075°C, respectively.

15-177, 1-1078, 12-671, 4-7-5856 and 37-158, respectively [18, 20–22]. In addition, there are some crystalline phases that are not yet identified. The heat treatment results in the coarsening of an already phase separated glass structure and crystallization of these phases. Furthermore, the treatment at the higher growth temperature of 1075°C induces the formation of a new crystalline phase, $CaSiO_3$ (Wollastonite; card number 42-550) [18], as shown in Fig. 2II (a–d) which is similar to that reported by De Aza and Luklinska [4].

We may compare the intensity of various peaks to estimate the effect of glass composition on the relative amounts of various phases. Specifically, Fig. 2I and II show the fraction of the various crystalline phases as a function of $CaF_2$ mol% and $T_x$. The amount of $Ca_5(PO_4)_3F$ increases with increasing $CaF_2$ content from 1 to 4 mol%. With further increase of $CaF_2$ content from 8 to 12 mol%, the intensity of peaks for the $Ca_5(PO_4)_3F$ crystalline phase starts decreasing, whereas the intensity of the peaks for the $Ca_5Si_2O_8F_2$ and $CaSiO_3$ phases increases.

### 3.2 Microstructure as a function of composition and heat + chemical treatment

Figures 3, 4 and 5 show the development of porous structure with increasing fluorine content when the heat treated samples of the 48SxFGI and 48SxFGII glass-ceramic series are subjected to chemical etching in 0.3 N HCl at 85°C for 1 h. Figure 4 also includes insets of the

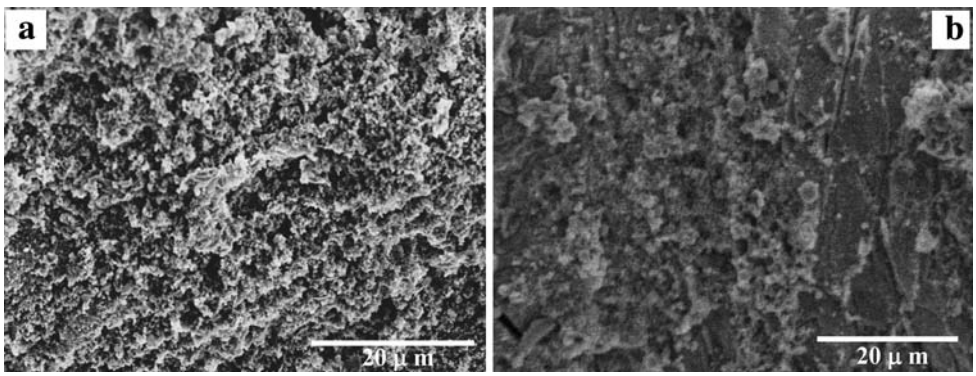


**Fig. 3** Low magnification SEM micrographs of the specimens after heat treatment and chemical leaching in 0.3 N HCl: **a** 48S4FGI, **b** 48S4FGII

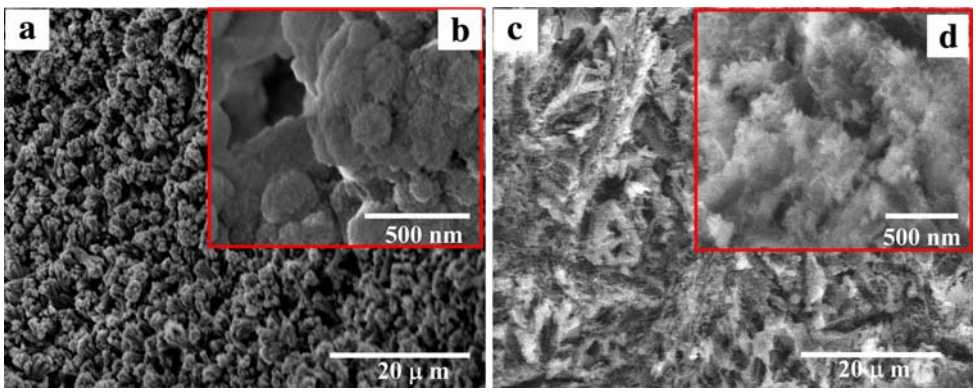


**Fig. 4** Low and high magnification SEM micrographs of the specimens after heat treatment and chemical leaching in 0.3 N HCl: **a–b** 48S10FGI, **c–d** 48S10FGII

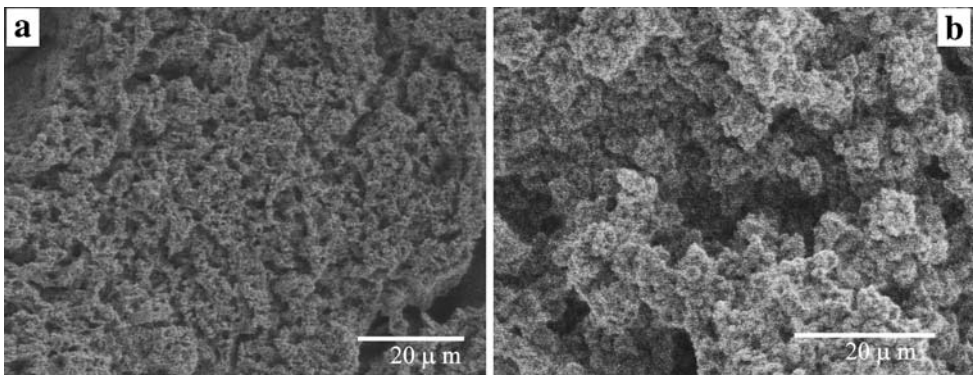


**Fig. 5** Low magnification SEM micrographs of the specimens after heat treatment and chemical leaching in 0.3 N HCl: **a** 48S12FGI, **b** 48S12FGII

microstructure at a much higher magnification, where nanoscale pores can be seen readily. It is clear from the micrographs obtained at relatively low and high magnifications that the present melt-quench-heat-etch method has produced a structured network of interconnected nano-macro porosity—in Fig. 4 we show but only one example of our nano-macroporous glass-ceramic series. The detailed process for the creation of multi-modal nano-macro interconnected porosity in these samples is similar to that observed in fluorine-free composition investigated previously [14]. It is observed from a comparison of micrographs of 48SxFGI versus 48SxFGII glass series in Figs. 3, 4 and 5 that the macropore number density in 48SxFGI samples is higher than that in the 48SxFGII samples i.e. the number of macropores/volume decreases when the heat treatment temperature is increased from 750 to 1075°C. In addition, note that the macropore density of both 48SxFGI and 48SxFGII series increases with increasing $CaF_2$ content from 4 to 10 mol% (micrographs for intermediate compositions are not shown here). However, the macropore number density decreases upon increasing the $CaF_2$ concentration from 10 to 12 mol%. The multi-modal nano-macro interconnected porosity in the heat + chemical treated sample 48S8FGI is confirmed by mercury porosity data in Fig. 6.

The XRD patterns of the heat + chemical treated porous 48SxFGI and 48SxFGII glass-ceramic samples are shown in Fig. 7I and II, respectively. We find that the crystalline phases in 48SxFGI and 48SxFGII samples did not leach out completely but only partially. In particular, the two crystalline phases $Na_2Ca_2Si_3O_9$ and $Ca_5(PO_4)_3F$ are more resistant to leaching and hence observed predominantly, compared to other crystalline phases ($Ca_4P_6O_{19}$, $Na_2CaSi_3O_8$, $Ca_5Si_2O_8F_2$, and $CaSiO_3$) after the leaching chemical treatment. It is worth noting again that there are some crystalline phases that could not be identified.

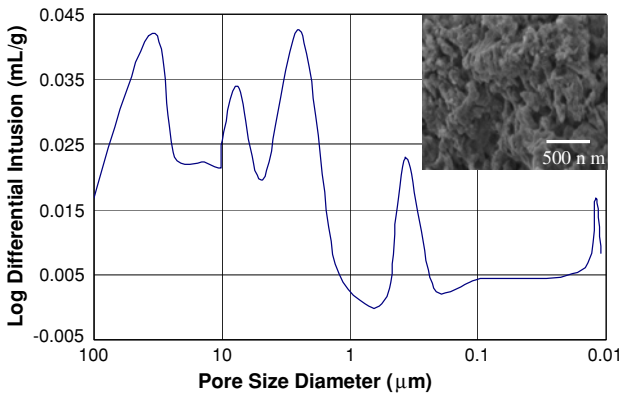


**Fig. 6** Pore size distribution and high magnification SEM micrograph for 48S8FGI glass-ceramic after chemical treatment

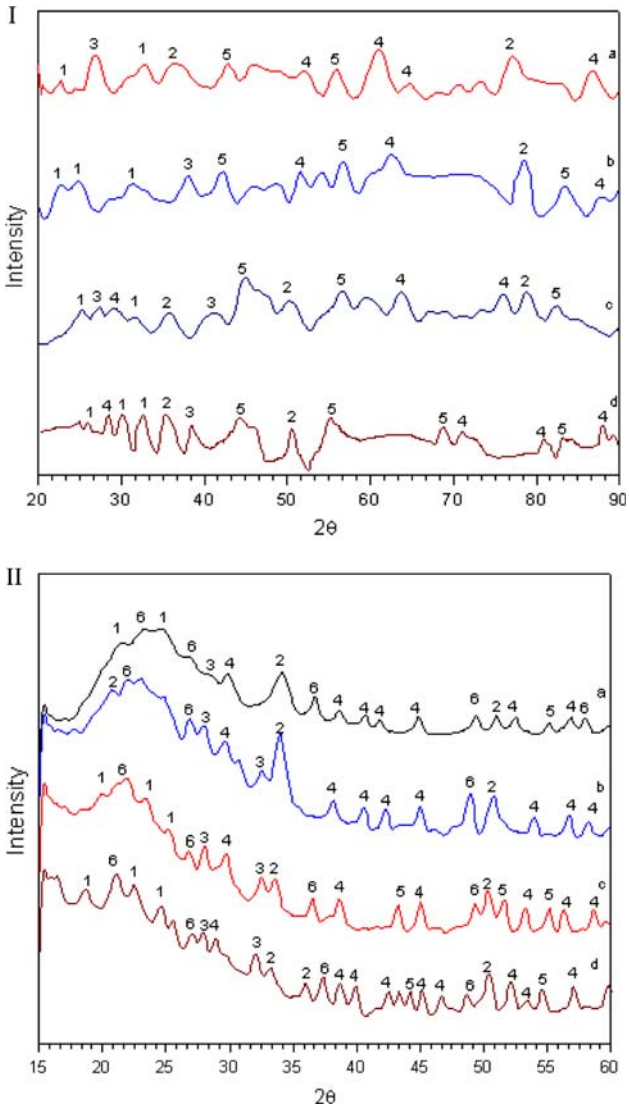


**Fig. 7** X-ray diffraction patterns of the specimens after heat treatment and chemical leaching: **I**: (a) 48S4FGI, (b) 48S8FGI, (c) 48S10FGI, (d) 48S12FGI. **II**: (a) 48S4FGII, (b) 48S8FGII, (c) 48S10FGII, (d) 48S12FGII. (1) $Ca_4P_6O_{19}$, (2) $Na_2Ca_2Si_3O_9$, (3) $Na_2CaSi_3O_8$, (4) $Ca_5(PO_4)_3F$, (5) $Ca_5Si_2O_8F_2$, and (6) $CaSiO_3$

### 3.3 Formation of HA layer as a function of composition and heat treatment

Figure 8 shows SEM micrographs of the 48SxFGI series of glass-ceramics for $x = 1$, 8, 10 and 12) after soaking in SBF for 3 days. We find that a layer is formed on the surface of all the samples of both 48SxFGI and 48SxFGII series (photographs for the 48SxFGII samples are not presented in Fig. 8). Presumably, the so formed layer is HA and enriched in Ca and P. It covers the whole surface of the 48SxFGI and 48SxFGII samples. Note that the deposited large particles aggregate on the surface of 48SxFGI and 48SxFGII samples with $x = 1$, 8 mol% $CaF_2$. By comparison, smaller particles aggregate on the surface of

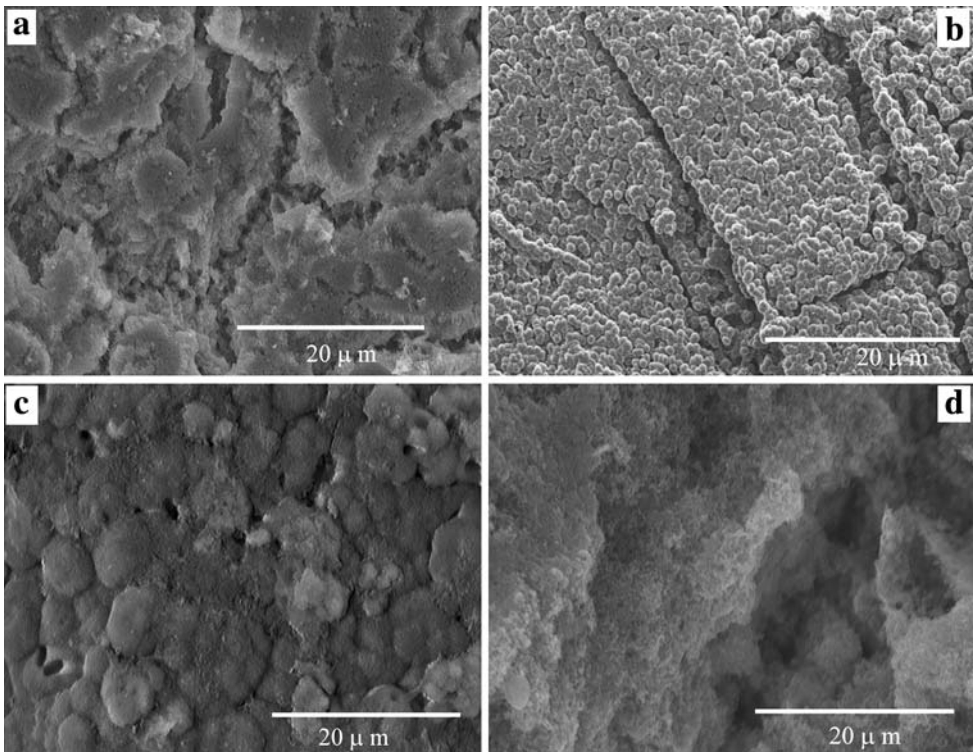


**Fig. 8** SEM micrographs of heat treated specimens after soaking for 3 days in SBF: (**a**) 48S1FGI, (**b**) 48S8FGI, (**c**) 48S10FGI, (**d**) 48S12FG1

48SxFGI and 48SxFGII samples with $x = 10$ and 12 mol% $CaF_2$.

The composition of the layer formed on the surface of glass-ceramic samples is determined by EDX and XRD analysis. Figure 9 shows EDX spectra for the surface layer on various samples. By comparing Fig. 9(a, b) with (c–e), and also Fig. 9(f, g) with (h–j), we note that the intensity of two key elements, Ca and P, increases with increasing $CaF_2$ for the glasses initially made with $x = 1$–4 mol%. For the higher $x = 8$–10 mol% $CaF_2$ content, an opposite trend is observed (Fig. 9(c, d) and (h, i)). For $x =$ 10–12 mol% $CaF_2$ we also note that the intensity of P decreases (Fig. 9(d, e) and (i, j)). It seems that the underlying phases and their distribution strongly determine the formation of HA layer on the surface of our glass-ceramic samples. For example, the higher peak intensity of P and Ca in the surface layer on 48SxFGI (Fig. 9a–c and 48SxFGII (Fig. 9f–h) glass-ceramic samples containing 1–8 mol% $CaF_2$ correlates with the predominance of $Na_2Ca_2Si_3O_9$, $Na_2CaSi_3O_8$, and $Ca_5(PO_4)_3F$ crystalline phases as determined from the XRD patterns in Fig. 2I (a–c) and II (a, b). It is known that $Na_2Ca_2Si_3O_9$ and $Na_2CaSi_3O_8$ strongly enhance the bioactivity of glass-ceramics [12, 18, 23]. At the same time, the crystal structure of crystalline $Ca_5(PO_4)_3F$ (fluorapatite) is very similar to the structure of HA [24]. Thus, fluorapatite crystalline phase can be considered as a seed or nucleation center for the formation of HA phase.

On the other hand, the decreasing concentration of two key elements (P and Ca) in the surface layer on 48SxFGI and 48SxFGII glass-ceramics containing (8–10) mol% $CaF_2$ (Fig. 9(c, d), (h, i)) and also decreasing concentration of P with higher (10–12) mol% $CaF_2$ (Fig. 9(d, e), (i, j)) may be correlated to the decrease of $Na_2Ca_2Si_3O_9$, $Na_2CaSi_3O_8$, $CaSiO_3$ and $Ca_5(PO_4)_3F$ crystalline phases and/or the increase of the $Ca_5Si_2O_8F_2$ phase—see XRD patterns in Fig. 2I (d, e) vs. II (c–d). From Figs. 2, 8 and 9 we find a correlation between the presence of $Na_2Ca_2Si_3O_9$, $Na_2CaSi_3O_8$, and/or $Ca_5(PO_4)_3F$ crystalline phases and an enhanced formation of HA layer on the surface of our glass-ceramic samples. From the present data it is difficult to establish the precise relative efficacy of these phases for the formation of HA layer. Nonetheless, we can conclude that the other crystalline phases, viz. $Ca_5Si_2O_8F_2$ and $CaSiO_3$ are much less effective for promoting the formation of HA than the $Na_2Ca_2Si_3O_9$, $Na_2CaSi_3O_8$, and $Ca_5(PO_4)_3F$ phases.

It is important to note that the $CaSiO_3$ crystalline phase is formed only in samples subjected to higher crystal growth temperature (1075°C). Its fraction decreases with increasing $CaF_2$ concentration in glass from 8 to 12 mol% (see Fig. 2II(b–d)). In addition, the fraction of $Ca_5Si_2O_8F_2$ phase increases with increasing $CaF_2$ content from 10 to 12 mol% (see Fig. 2II(c, d)). So for the formation of HA, the growth heat treatment at 750°C is more effective than the one at 1075°C. Furthermore, the addition of 4–8 mol%

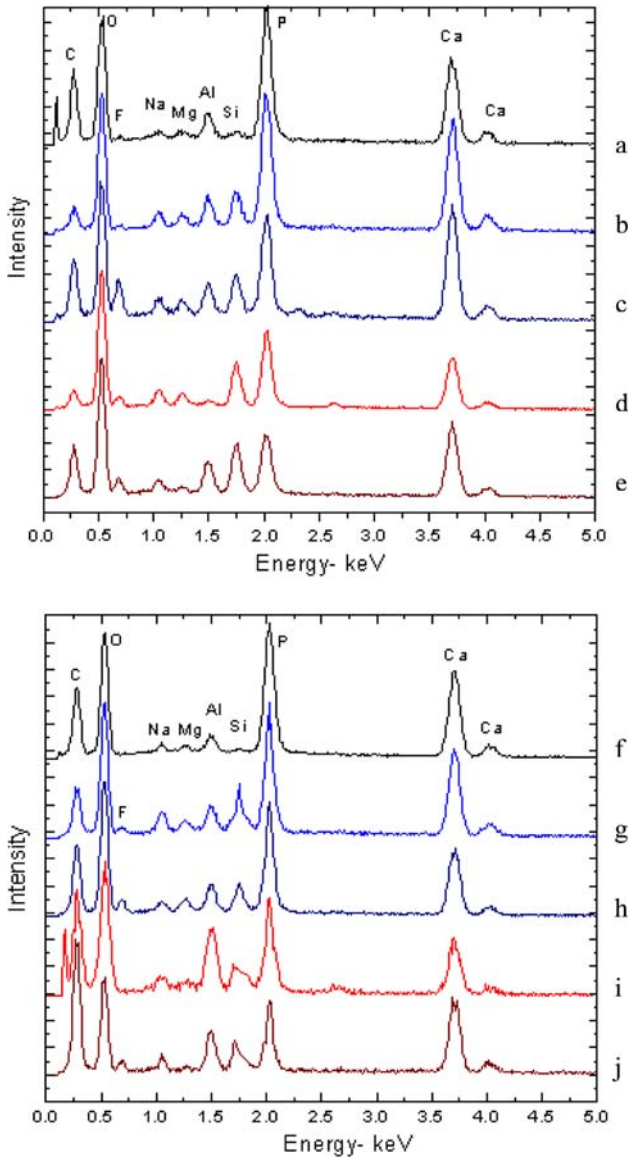


**Fig. 9** EDX spectra of heat treated specimens (same as in Fig. 8) after soaking for 3 days in SBF: (a) 48S1FGI, (b) 48S4FGI, (c) 48S8FGI, (d) 48S10FGI, (e) 48S12FGI, (f) 48S1FGII, (g) 48S4FGII, (h) 48S8FGII, (i) 48S10FGII, (j) 48S12FGII

$CaF_2$ is more helpful for the formation of HA than its higher content of 10–12 mol%. In short, the best parameters for enhancing the formation of HA layer are: initial composition that contains 4–8 mol% $CaF_2$ and crystal growth temperature of 750°C for our 48S based glass-ceramics.

### 3.4 Formation of HA layer as a function of composition and heat + chemical treatment

Figure 10 shows SEM micrographs of the 48SxFGI porous glass-ceramics, which were subjected to soaking in SBF for 3 days. Note that an HA layer is formed on the surface of the porous glass-ceramics samples 48SxFGI and 48SxFGII (micrographs for the latter series are not shown here). Many spherical shaped HA particles formed aggregations on the 48SxFGI and 48SxFGII porous glass-ceramic samples with $x = 1$–8 mol%, such as shown in Fig. 10(a, b) for 48SxFGI samples. Their number density is significantly

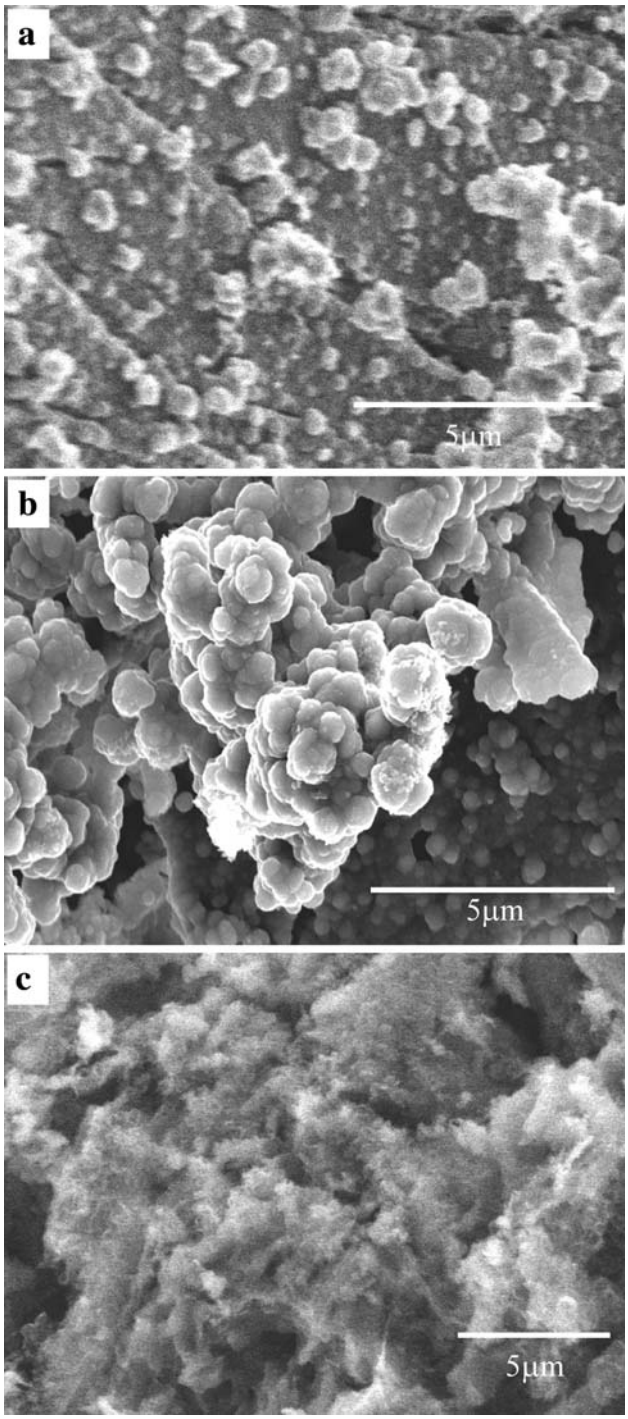


**Fig. 10** SEM micrographs of chemically treated glass-ceramic after soaking for 3 days in SBF: **a** 48S1FGI, **b** 48S8FGI, **c** 48S10FGI

higher than that on the surface of samples with $x =$ 10–12 mol% (see, for example, Fig. 10c).

Figure 11 shows EDX spectra for the 48SxFGI and 48SxFGII porous glass-ceramics shown in Fig. 10. The intensity of P and Ca peaks for the samples with 1 to 8 mol% $CaF_2$ in Fig. 11(a–c) and (f–h) is larger than that for the samples with 10–12 mol% $CaF_2$ (see Fig. 11(d, e) and (i, j)). Note from the XRD patterns in Fig. 7 for the 48SxFGI and 48SxFGII samples after the leaching treatment that the two predominant crystalline phases are $Na_2Ca_2Si_3O_9$ and $Ca_5(PO_4)_3F$ compared to $Ca_4P_6O_{19}$, $Na_2CaSi_3O_8$, $Ca_5Si_2O_8F_2$, and $CaSiO_3$ as the minor phases.

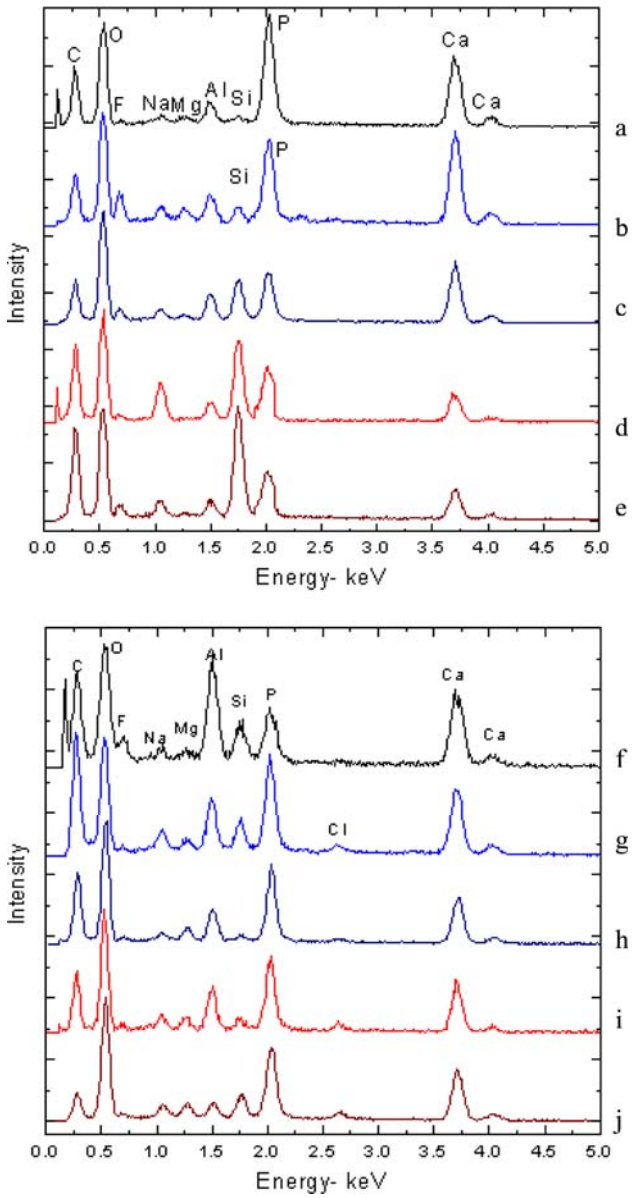


**Fig. 11** EDX spectra of chemically treated glass-ceramic samples after soaking for 3 days in SBF: (a) 48S1FGI, (b) 48S4FGI, (c) 48S8FGI, (d) 48S10FGI, (e) 48S12FGI, (f) 48S1FGII, (g) 48S4FGII, (h) 48S8FGII, (i) 48S10FGII, (j) 48S12FGII

Therefore, we infer that it is predominantly the existence of $Na_2Ca_2Si_3O_9$ and $Ca_5(PO_4)_3F$ that causes the enhancement of HA formation on the surface of 48SxFGI and/or 48SxFGII porous glass-ceramic samples (see Fig. 11(a–c) and (f–h) for glasses containing 1–8 mol% $CaF_2$). Therefore, we have avoided inasmuch as possible the leaching of the $Na_2Ca_2Si_3O_9$ and $Ca_5(PO_4)_3$ F crystalline phases from our glass-ceramics. By comparison, the spectra marked (d, e) and (i, j) in Fig. 11 show a decrease in the intensity of the peaks for P and Ca from the samples containing 10–12 mol% $CaF_2$, but it is not significantly smaller than that for the samples with $x =$ 1–8 mol% $CaF_2$.

Figures 3, 4, 5 show that the density of pores in 48SxFGI and 48SxFGII porous glass-ceramic samples increases with increasing $CaF_2$ content within $x =$ 4–10 mol%. Therefore, it appears that the multi-modal porosity in 48SxFGI and 48SxFGII porous glass-ceramics with $x =$ 4–10 mol% $CaF_2$ would allow the SBF to infiltrate the material freely and permit a more efficient transport of ions to and from the reactive surface than through the samples with larger $x$. Clearly, it is very important to balance the pore density vs. the leached amount of useful $Na_2Ca_2Si_3O_9$ and $Ca_5(PO_4)_3F$ phases.

We find that the HA layer covers the whole surface of 48S4FGI glass-ceramic samples, both solid and porous, after soaking for 7 days in SBF (SEM micrographs are not presented here). The nature of this layer on the surface of these samples is determined from their XRD patterns shown in Fig. 12. The location of diffraction peaks matches with the main peaks of HA crystal mentioned in PDF card number 09-0432 and is similar to that found by Peitl et al. [10]. Overall the intensity and sharpness of the diffraction peaks of HA layer after soaking in SBF for 7 days is greater than that formed after soaking for 3 days. On the other hand, the intensity of diffraction peaks for the HA layer formed on 48S4FGI solid and porous glass-ceramic samples after soaking for 7 days in SBF is nearly the same, see Fig. 12(I-c, II-c). It means that our processing parameters have been optimized with respect to the creation of multi-modal porosity and the formation of HA layer on this composition [12].

The surface layer formed on the porous 48S4FGI glass-ceramic sample after soaking in SBF for 1, 3 or 7 days is further confirmed to be hydroxy apatite by FT-IR spectroscopy, as shown in Fig. 13. The bands centered at 420, 460 $cm^{-1}$ (Si–O–Si bend) [25, 26] and 670, 750 $cm^{-1}$ (Si–O–Si symmetric stretch) [25–27] are related to the amount of silica present in the HA layer. The intensity of these bands (Si–O–Si) increases with increasing soaking time in SBF. On the other hand, the presence of phosphate group in the surface crystalline phase is confirmed by the presence of bands at 565 and 600 $cm^{-1}$ [27, 28]. The latter band representing P–O–P bending vibrations of $PO_4^{3-}$

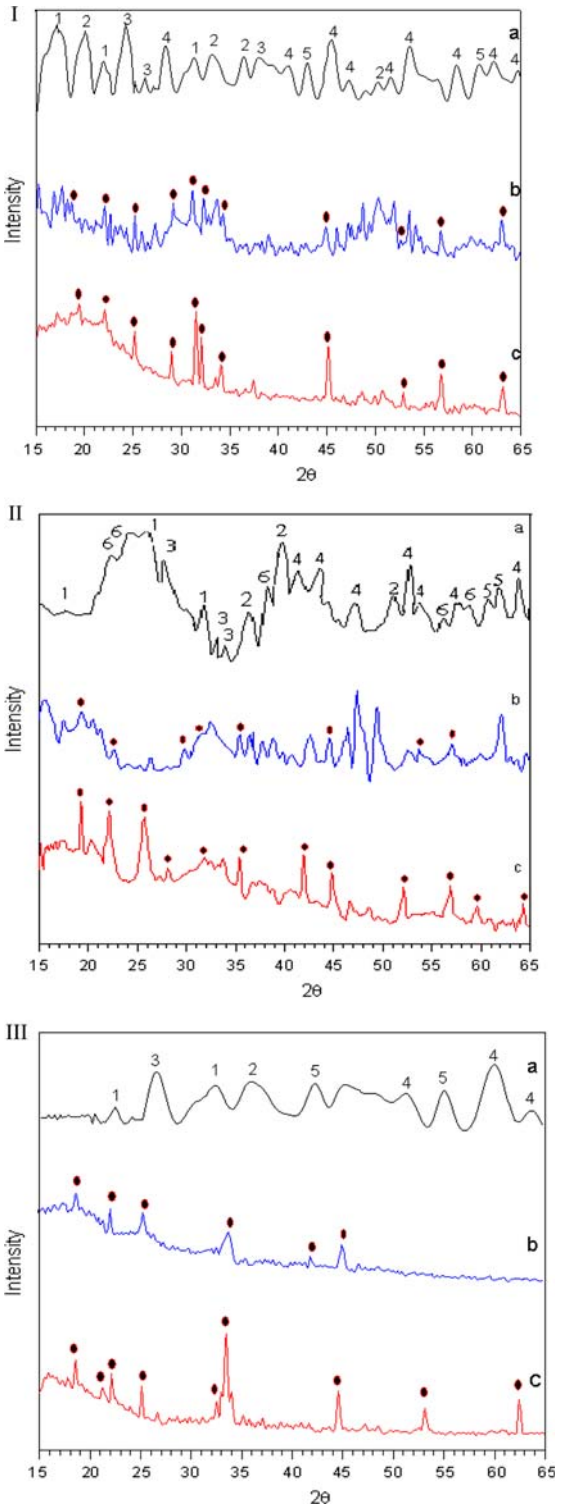


**Fig. 12** X-ray diffraction patterns of: **I** heat treated specimens [48S4FGI] after soaking in SBF for: (a) 0 h, (b) 3 days, and (c) 7 days. **II** heat treated specimens [48S4FGII] after soaking in SBF for: (a) 0 h, (b) 3 days, and (c) 7 days. **III** heat + chemically treated glass-ceramic specimens [48S4FGI] after soaking in SBF for: (a) 0 h, (b) 3 days, and (c) 7 days. (1)$Ca_4P_6O_{19}$, (2) $Na_2Ca_2Si_3O_9$, (3) $Na_2CaSi_3O_8$, (4) $Ca_5(PO_4)_3F$, (5) $Ca_5Si_2O_8F_2$, (6) $CaSiO_3$, •) $Ca_5(PO_4)_3(OH)$

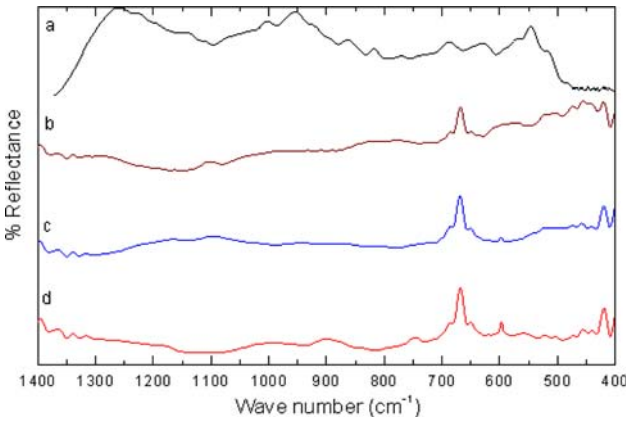


**Fig. 13** FTIR spectra of chemically treated glass-ceramic specimens [48S4FGI] after soaking in SBF for: (a) 0 h, (b) 1 day, (c) 3 days, and (d) 7 days

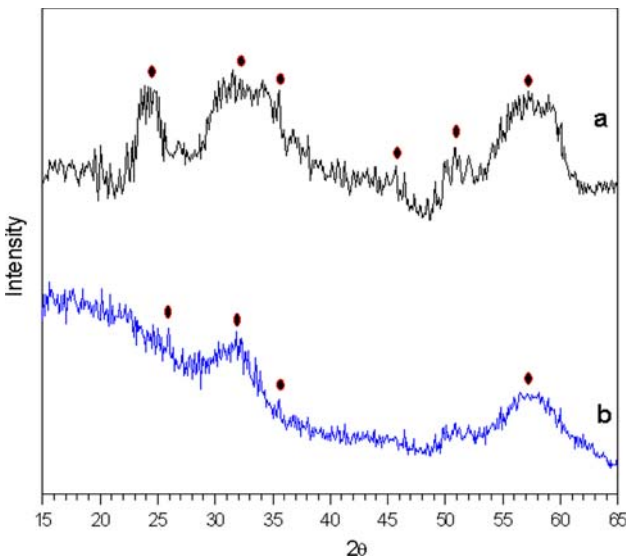


**Fig. 14** X-ray diffraction patterns for (a) 48S4F glass, (b) 48S glass after soaking in SBF for 7 days

tetrahedra in crystalline calcium phosphate [29] increases with increasing soaking time in SBF. Therefore, it appears that with increasing soaking time in SBF there is a formation of $SiO_2$-rich layer, which induces heterogeneous nucleation of hydroxy apatite. Once apatite nuclei are formed, they grow with time on the surface of our porous glass-ceramics.

### 3.5 Effect of fluoride ions on the formation of HA on glass surface

To establish the role of $F^-$ ions in the formation of HA, we have compared the XRD patterns for the 48S and 48S4F glass samples after soaking in SBF for 7 days. Figure 14 shows that the diffraction peaks for surface layer on 48S4F glass are stronger than those for the layer on 48S glass.

This simple comparison suggests that the presence of fluoride ions is likely to enhance the bioactivity of soda-lime phosphosilicate glass.

## 4 Conclusion

There has existed a controversy in the literature about the effect of crystallization of bioactive glass on the formation of hydroxyl apatite layer. Our results indicate that there are four important parameters, which may affect the formation of HA layer on the surface of nano-macroporous soda-lime phosphofluorosilicate samples prepared by the melt-quench-heat-etch method. These parameters are: initial glass composition, temperature of crystallization, type of crystalline phases and leached amount of useful $Na_2Ca_2Si_3O_9$ and $Ca_5(PO_4)_3F$ phases. The present heat treatment produces multi-phase glass-ceramics, which upon chemical leaching yield a highly interconnected porous microstructure. This tendency of interconnected macroporosity on the scale of 10 s of microns is due to the growth and coalescence of the crystalline regions, whereas nanoscale interconnected porosity is retained by the initial spinodal phase separation in the melt-quenched glass.

The soaking of glass-ceramics in SBF shows the formation of HA on the surface of both the heat-treated glass-ceramics and chemically etched porous glass-ceramics. The formation of HA and hence bioactivity is significantly influenced by the mol% of $CaF_2$ in the initial glass composition. Furthermore, the presence of $Na_2Ca_2Si_3O_9$, $Na_2CaSi_3O_8$, and especially $Ca_5(PO_4)_3F$ crystalline phases in glass-ceramics also promotes the formation of HA layer and hence their bioactivity.

**Acknowledgement** This work was initiated and continued as an international collaboration with support from National Science Foundation (International Materials Institute for New Functionality in Glass (DMR-0409588) and Materials World Network (DMR-0602975) programs).

## References

1. Li N, Jie Q, Zhu S, Wang R. Preparation and characterization of macroporous sol–gel bioglass. Ceram Int. 2005;31:641–6.
2. Jones JR, Hench LL. Biomedical materials for new millennium: perspective on the future. Mater Sci Technol. 2001;17:891–900.
3. Lin FH, Hon MH. A study on bioglass ceramics in the $Na_2O$–$CaO$–$SiO_2$–$P_2O_5$ system. J Mater Sci. 1988;23:4295–9.
4. De Aza PN, Luklinska ZB. Effect of glass-ceramic microstructure on its in vitro bioactivity. J Mater Sci Mater Med. 2003;14:891–8.
5. Merolli A, Leaali PT, Guidi PL, Gabbi C. Comparison in in-vivo response between a bioactive glass and a non-bioactive glass. J Mater Sci Mater Med. 2000;11:219–22.
6. Thompson ID, Hench LL. Mechanical properties of bioactive glasses, glass-ceramics and composities. Proc Inst Mech Eng Part H: J Eng Med. 1998;212:127–36.
7. Holand W, Vogel W, Naumann K, Gummel J. Interface reactions between machinable bioactive glass-ceramics and bone. J Biomed Mater Res Part B. 1985;19:303–12.
8. Kokubo T. Bioactive glass ceramics: properties and applications. Biomaterials. 1991;12:155–63.
9. Li P, Yang Q, Zhang F, Kokubo T. The effect of residual glassy phase in a bioactive glass-ceramic on the formation of its surface apatite layer in vitro. J Mater Sci Mater Med. 1992;3:452–6.
10. Peitl O, Latorre G, Hench LL. Effect of crystallization on apatite-layer formation of bioactive 45S5. J Biomed Mater Res. 1996;30:509–14.
11. Vallet-Regi M, Roman J, Padilla S, Doadrio JC, Gill FJ. Bioactivity and mechanical properties of $SiO_2$–$CaO$–$P_2O_5$ glass-ceramics. J Mater Chem. 2005;15:1353–9.
12. Moawad HHM, Jain H. Fabrication of nano-macro porous soda-lime phosphosilicate bioactive glass by the melt-quench method. Ceram Eng Sci Proc: Developments in Porous, Biological and Geopolymer Ceramics. 2008;28(9):183–95.
13. Sepulveda P, Jones JR, Hench LL. Bioactive sol–gel foams for tissue repair. J Biomed Mater Res Part A. 2002;59:340–8.
14. Moawad HMM, Jain H. Creation of nano-macro interconnected porosity in bioactive glass-ceramic by the melt-quench-heat-etch method. J Am Ceram Soc. 2007;90:1934–6.
15. Marques AC, Jain H, Almeida RM. Sol–gel derived nano/macroporous monolithic scaffolds. Eur J Glass Sci Technol. 2007;48:65–8.
16. Nakanishi K, Minakuchi H, Soga N. Structure design of double-pore silica and its application to HPLC. J Sol–Gel Sci Technol. 1998;13:163–9.
17. Nakanishi K. Pore structure control of silica gels based on phase separation. J Porous Mater. 1997;4:67–112.
18. El-Batal HA, Azooz MA, Khalil EMA, Monem AS, Hamdy YM. Characterization of some bioglass-ceramics. Mater Chem Phys. 2003;80:599–609.
19. Elemer TH, Nordberg ME, Carrier GB, Korda EJ. Phase separation in borosilicate glasses as seen by electron microscopy. J Am Ceram Soc. 1970;53:171–5.
20. Brentrup GJ, Moawad HMM, Santos LF, Almedia RM, Jain H. Structure of $Na_2O$–$CaO$–$P_2O_5$–$SiO_2$ glass-ceramics with multimodal porosity. J Am Ceram Soc. 2009;92:249–52.
21. Peitl O, Zanotto ED, Hench LL. Highly bioactive $P_2O_5$–$Na_2O$–$CaO$–$SiO_2$ glass-ceramics. J Non-Cryst Solids. 2001;292:115–26.
22. Chen X, Hench LL, Greespan D, Zhong J, Zhang X. Investigation on phase separation, nucleation and crystallization in bioactive glass-ceramic containing fluorophlogopite and fluorapatite. Ceram Int. 1998;24:401–10.
23. Lin CC, Huang LC, Shen P. $Na_2CaSi_2O_6$–$P_2O_5$ based bioactive glasses. Part 1: elasticity and structure. J Non-Cryst Solids. 2005;351:3195–203.
24. Mathew M, Takagi S. Structures of biological minerals in dental research. J Res Natl Inst Stand Technol. 2001;106:1035–44.
25. Abo-Naf SM, El Batal FH, Azooz MA. Characterization of some glasses in the system $SiO_2$, $Na_2O \cdot RO$ by infrared spectroscopy. Mater Chem Phys. 2003;77:846–52.
26. Sitarz M, Handke M, Fojud Z, Jurga S. Spectroscopic studies of glassy phospho-silicate materials. J Mol Struct. 2005;744–747:621–6.
27. El Batal FH, Elkheshen A. Characterization of some glasses in the system $SiO_2$, $Na_2O \cdot RO$ by infrared spectroscopy. Mater Chem Phys. 2008;110:352–62.
28. Saiz E, Goldman M, Gomez-Vega JM, Tomsia AP, Marshall GW, Marshall SJ. In vitro behavior of silicate glass coatings on Ti6Al4V. Biomaterials. 2002;23:3749–56.
29. Pereira MM, Clark AE, Hench LL. Calcium phosphate formation on sol–gel-derived bioactive glasses in vitro. J Biomed Mater Res Part A. 1994;28:693–8.